Transitional Area of Ce^{4+} to Ce^{3+} in $Sm_xCa_yCe_{1-x-y}O_{2-\delta}$ with Various Doping and Oxygen Vacancy Concentrations: A GGA + *U* Study

WU Tong-Wei[1] (吴铜伟);JIA Gui-Xiao[1,2](贾桂霄);WANG Xiao-Xia[1] (王晓霞);LI Lei[1] (李磊);AN Sheng-Li[1,2](安胜利)

[1] *School of Materials and Metallurgy, Inner Mongolia University of Science and Technology, Baotou, Inner Mongolia* 014010, *China*;[2]*The Inner Mongolia Autonomous Region Key Lab of Novel Functional Ceramics and Devices, Baotou, Inner Mongolia* 014010, *China*

ABSTRACT In this work, we perform DFT + U periodic calculations to study geometrical and electronic structures and oxygen vacancy formation energies of $Sm_xCa_yCe_{1-x-y}O_{2-\delta}$ systems (x = 0.0312, 0.0625, 0.125 and 0.250; y = 0.0312, 0.0625, 0.125 and 0.250; δ = 0.0312, 0.0625, 0.125, 0.250 and 0.50) with different oxygen vacancy and doping concentrations. The calculated results show that the V_1-Sm^{3+}-V_2 structures where there is a position relationship of the face diagonal between V_1 and V_2 both nearest to Sm^{3+} have the lowest energy configurations. The study on electronic structures of the $Sm_xCa_yCe_{1-x-y}O_{2-\delta}$ systems finds that excess electrons arise from oxygen vacancies and are localized on *f*-level traps of their neighbor Ce, and Ca^{2+} and Sm^{3+} co-doping effectively restrains the reduction of Ce^{4+}. In order to avoid the existence of Ce^{3+}, x and y must be both larger than 0.0625 as δ = 0.125 or δ must be smaller than 0.125 as $x = y$ = 0.0625. The Ce^{3+}/Ce^{4+} change ratio k has an obvious monotonous increase with increasing the vacancy oxygen concentration. The introduction of Sm^{3+} decreases k. In addition, the doped Sm^{3+} can restrain the reduction of Ce^{4+} when the V_1-Sm^{3+}-V_2 structure with a face diagonal position relationship in lower reduced atmosphere exists. It need be pointed out that the $Sm_{0.25}Ce_{0.75}O_{1.5}$ system should be thought of as a Sm-doped Ce_2O_3 one.

Keywords: cerium oxide;oxygen vacancies; doping; electronic structures; GGA+*U*;

DOI: 10.14102/j.cnki.0254-5861.2011-1715

1 INTRODUCTION

CeO_2-based materials are important in solid oxide fuel cells (SOFC)[1-3] due to their high ionic

conductivity. Pure CeO_2 is a mixed ionic and electronic conductor. When a neutral oxygen vacancy is built in CeO_2, two excess electrons left behind will be localized on the *f*-level traps of two neighbor Ce, namely, formally Ce^{4+} is reduced to Ce^{3+}[Ce'_{Ce}][4-6]. Therefore, to improve its ionic conductivity and decrease its electronic conductivity[7-15], CeO_2 is commonly doped with alkaline earth or rare earth metals such as Ca^{2+}, Gd^{3+}, Sm^{3+} and La^{3+} or their co-doping.

Now, ionic and electronic conductivities of CeO_2 have been widely studied[7-18]. Mogensen's study on Ca or Gd single-doped CeO_2 systems found that the conduction carrier was related with atmosphere[18]. The conductivity measured in air is regarded as being ionic and the electronic conductivity contribution is negligible, and ionic conductivity (σ_i) and electronic conductivity (σ_e) are connected with oxygen partial pressure (P_{O_2}) in reduced atmosphere[18]. The highest σ_i of CeO_2 doped with 20mol% Ca is 0.209 S/cm at H_2 atmosphere at 850 ℃, larger than that in air[19]. $Ce_{1-x}M_xO_{2-\delta}$ (M = Gd^{3+} or Sm^{3+}) at x = 0.15, 0.2 and $(Ce_{0.8}Sm_{0.2})_{1-0.05}Ca_{0.05}O_{2-\delta}$ compounds have the largest ionic conductivity[7-9], and the conductivity of the latter is 0.126 S/cm at 800 ℃ in air. In addition, the ionic radii and valence of dopants[16-20], oxygen vacancy and dopant concentrations[21], and dopant-vacancy and vacancy-vacancy defect associations[22] which decrease the number of mobile vacancies available, also affect the ionic conductivity of CeO_2.

Theoretically, the distributions of oxygen vacancies and dopants[23], their formation energies[24], geometric and electronic structures[25] and oxygen ionic migration energies of CeO_2 systems[15, 25, 26] have been investigated at the atomic level. CeO_2 systems with Sm^{3+} among rare earth metals and Ca^{2+} among alkaline earth metals have the smallest oxygen ionic migration energies[25, 27] and their doping can effectively restrain the electronic conductivity. Theoretical[9] and experimental[28, 29] studies showed that Ca^{2+} and Sm^{3+} co-doping could better improve the ionic conductivity. Effects of different oxygen vacancy and doping concentrations on the distributions of oxygen vacancies, dopants and Ce^{3+} of the CeO_2 systems are investigated. Murgida's study[30] showed that the oxygen vacancy concentration affected the distribution of Ce^{3+} and excess electrons preferred to be localized in the cation sites such that the mean Ce^{3+} coordination number was maximized, and two vacancies were inclined to be second-neighboring. For doped $CeO_{2-\delta}$, our and other studies found that dopants preferred to occupy the nearest neighbor (NN) and next-nearest neighbor (NNN) positions relative to the oxygen vacancy[20, 25]. Independent with oxygen vacancy and doping concentrations, Ce^{3+} is distributed around the nearest neighbor oxygen vacancy[30-32].

However, a systematically theoretical study on Ce^{3+}/Ce^{4+} electronic properties of CeO_2 with different

oxygen vacancy and doping concentrations is absent. As is well known, Ca and Sm doping can effectively restrain the reduction of Ce^{4+} to Ce^{3+} and the doped CeO_2 has the largest ionic conductivity. Hence, in order to better understand the effects of different oxygen vacancy and Ca-, Sm-doping concentrations on the electronic structures (Ce^{3+}/Ce^{4+}) of CeO_2 systems, in the work, we select various numbers of oxygen vacancies or Ca and Sm dopants in the same supercell to obtain a series of vacancy and doping concentrations. Ultimately, this work would plot transitional area of Ce^{4+} to Ce^{3+} and the Ce^{3+}/Ce^{4+} change ratio k under different oxygen vacancy and doping concentration conditions.

2 MODELS AND COMPUTATIONAL DETAILS

2. 1 Models

CeO_2 has a fluorite-type structure (*Fm*3*m* space group) with one formula unit per primitive unite cell[25]. In this work, we considered a number of oxygen vacancies or dopants of Ca^{2+} and Sm^{3+} to produce various oxygen vacancy and doping concentrations in a 2×2×2 supercell, namely, $Sm_xCa_yCe_{1-x-y}O_{2-\delta}$ systems with various x, y and δ (x = 0.0312, 0.0625, 0.125 and 0.250; y = 0.0312, 0.0625, 0.125 and 0.250; δ = 0.0312, 0.0625, 0.125, 0.250 and 0.50) were considered, see Table 1. When the doping concentration is larger than 0.30, $Sm_xCa_yCe_{1-x-y}O_{2-\delta}$ systems were not doping but alloying ones. However, for convenience with description in the work, we would unify them to name as doping ones.

Doped atoms are uniformly distributed in a 2×2×2 supercell to obtain systems with various doping concentrations. Hooper's study[33] on Sm-doped CeO_2 systems found that the dopant-vacancy interaction was a hybrid NN/NNN mixture distribution as the Sm^{3+} concentrations increased and more NN distributions were the most favored. Our previous studies found that the first oxygen vacancy (V_1) was the nearest to the dopant (NN)[20, 25]. Here, the same structure model is used. For the CeO_2 systems where the number of the oxygen vacancy nearest to one Sm^{3+} is more than one, these vacancies are chosen according to the rule of the NN distribution, namely, the second oxygen vacancy nearest to one Sm^{3+} is introduced and named as V_2. Thus, V_1 and V_2 would have three distinct position relationships in the cube of eight coordinated O^{2-} for one Sm^{3+}, namely, the side one in Fig. 1a, the face diagonal one in Fig. 1b and the body diagonal one in Fig. 1c. Calculation results show that the structures with the face diagonal relationship between V_1 and V_2 are the most stable, consistent with the case of pure CeO_2 systems with double oxygen vacancies[8]. For Ca-doped CeO_2

systems, the models where Ca^{2+} has a NN or NNN distribution relationship with one oxygen vacancy are considered.

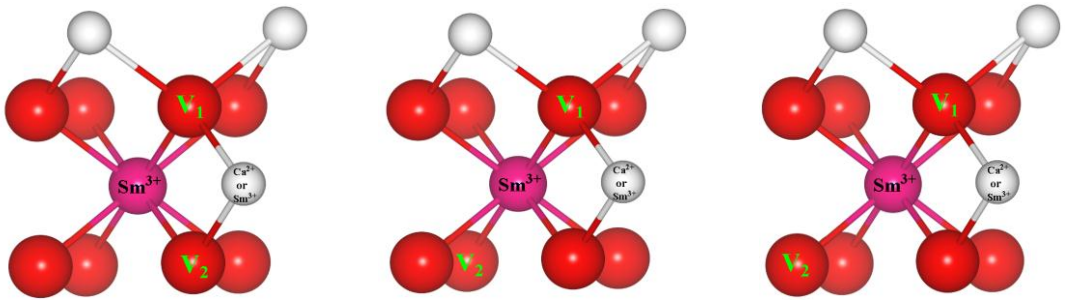

(a) (b) (c)

Fig. 1. Geometric structures of $Sm_{0.25}Ca_{0.25}Ce_{0.5}O_{2-\delta}$ or $Sm_{0.5}Ce_{0.5}O_{2-\delta}$ systems with V_1 and V_2. Red spheres note O, white ones note Ce, and the pink ones note one Sm^{3+}. There is a similar notation in the following figures

2. 2 Computational details

All calculations were performed by a Vienna *ab initio* simulation package (VASP)[34]. Ce5*s*5*p*6*s*4*f*5*d*, O2*s*2*p*, Ca3*s*3*p*4*s* and Sm5*s*5*p*6*s*4*f*5*d* were treated as valence electrons. Structures were relaxed until forces on each ion were below 0.02 eV/Å and the total energy was converged within 1×10^{-4} eV. A plane-wave cut off energy of 400 eV, a 3×3×3 Monkhorst-Pack k point mesh and a Gaussian smearing parameter of 0.20 eV were used.

The standard DFT formulation usually fails to describe strongly the correlated electrons due to a deficient treatment of electron correlation. This limitation can be corrected by using a DFT + U method, where the introduction of a Hubbard parameter *U* modifies the self-interaction error and enhances the description of the correlation effects[35]. This methodology has been widely used in reduced CeO_2 systems[6, 8, 32, 35]. Theoretical work showed that the *U* value for Ce should be larger than 5.0 eV[25, 26, 34]. In this work, we used the *U*-value of 6.0 eV for Ce and *U*-value of 8.0 eV and *J*-value of 0.65 eV for Sm, consistent with the other work[35-47]. The exchange-correlation effects were described with the Perdew Burke Ernzerhof (PBE) functional within the generalized gradient approximation (GGA)[36]. The calculated crystal lattice constant from the GGA + *U* method is 5.48 Å, in agreement with the experiment value of 5.41 Å[48].

The formation energies of oxygen vacancies E_{Vo} for $CeO_{2-\delta}$ systems, $E_{Vo\text{-}Sm}$ for $Sm_xCeO_{2-\delta}$ systems and $E_{Vo\text{-}CaSm}$ for $Sm_xCa_yCeO_{2-\delta}$ systems can be defined as

$$E_{V_O-(Sm,CaSm)} = E[X] + \frac{p}{2}E[O_2] - E[Y] \quad (1)$$

where $E[X]$ and $E[Y]$ are total energies of pure or doped CeO_2 systems with and without oxygen vacancies, respectively. $E[O_2]$ is the energy of one O_2 molecule set in a 10Å × 10Å × 10Å supercell, and p is the number of oxygen vacancies.

3 RESULTS AND DISCUSSION

3. 1 Geometric structures

Model structures with the lowest energies are obtained. The V_1-Sm^{3+}-V_2 structures where there is a diagonal position relationship of the face between V_1 and V_2 both nearest to Sm^{3+} have the lowest energy configurations, consistent with the case of pure CeO_2 systems with double oxygen vacancies[8]. The introduction of Sm^{3+}, Ca^{2+} and oxygen vacancies into CeO_2 can produce obvious geometric distortions, consistent with the other work[25]. Geometric structures of $CeO_{1.9688}$, $Sm_{0.0312}Ce_{0.9688}O_{1.9688}$, $Sm_{0.0312}Ce_{0.9688}O_{1.9375}$, $Sm_{0.0312}Ca_{0.0312}Ce_{0.9376}O_{1.9688}$ and $Sm_{0.0312}Ca_{0.0312}Ce_{0.9376}O_{1.9375}$ systems as examples are displayed in Fig. 2. Geometric structures of $Sm_xCa_yCe_{1-x-y}O_{2-\delta}$ with other oxygen vacancy and doping concentrations have a similar geometric distortion.

It is well known that the oxygen vacancy is an area of effective positive potential, hence, the neighboring O^{2-} move toward the vacancy, and the neighboring Ce^{4+} move away from the vacancy. From Fig. 2a of the $CeO_{1.9688}$ system, we can see that three of four O^{2-} near the oxygen vacancy move toward it and another O^{2-} moves away from it. From the following electronic structures (see detail discussion on electronic structures), it is known that this O^{2-} is bridged by two Ce^{3+} which have larger negative potential than that of Ce^{4+}. From Fig. 2b of the $Sm_{0.0312}Ce_{0.9688}O_{1.9688}$ system, it is similar to the $CeO_{1.9688}$ system in Fig. 2a and the difference is that one of two Ce^{3+} is Sm^{3+}, namely, the neighboring O^{2-} move toward the vacancy, and the neighboring Ce^{4+} and Sm^{3+} move away from the vacancy. From Fig. 2c of the $Sm_{0.0312}Ce_{0.9688}O_{1.9375}$ system, we can see that the movements of four O^{2-} toward two vacancies and two O^{2-} toward Sm^{3+} resulted from the common attraction of V_1 and V_2 to O^{2-}, namely, an O^{2-} bridged by Sm^{3+} and Ce^{3+} is not repelled, different from the systems with one oxygen vacancy. From Fig. 2d of the $Sm_{0.0312}Ca_{0.0312}Ce_{0.9376}O_{1.9688}$ system, four O^{2-} near the oxygen vacancies can be driven toward the vacancy and the neighboring Ce^{4+} move away from the vacancy. The $Sm_{0.0312}Ca_{0.0312}Ce_{0.9376}O_{1.9375}$ system in Fig. 2e is similar to the $Sm_{0.0312}Ce_{0.9688}O_{1.9375}$ system in Fig. 2c.

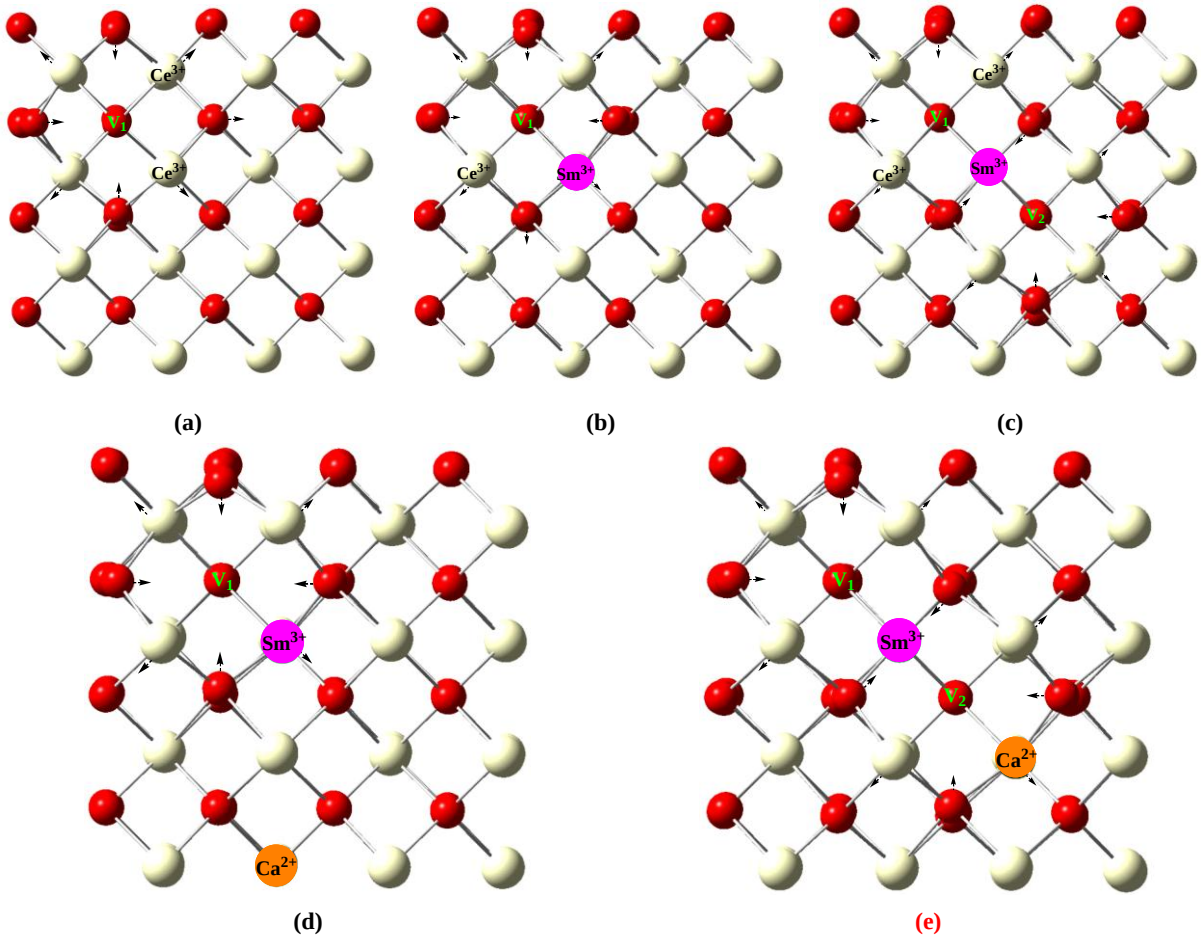

Fig. 2. Optimized geometric structures of the $CeO_{1.9688}$ (a), $Sm_{0.0312}Ce_{0.9688}O_{1.9688}$ (b), $Sm_{0.0312}Ce_{0.9688}O_{1.9375}$ (c), $Sm_{0.0312}Ca_{0.0312}Ce_{0.9376}O_{1.9688}$ (d) and $Sm_{0.0312}Ca_{0.0312}Ce_{0.9376}O_{1.9375}$ (e) systems. Arrow directions indicate moving ones of ions

3. 2 Oxygen vacancy formation energies

Table 1. Oxygen Vacancy Formation Energies (Unit: eV) of E_{Vo} for $CeO_{2-\delta}$, $E_{Vo\text{-}Sm}$ for $Sm_xCe_{1-x}O_{2-\delta}$ and $E_{Vo\text{-}CaSm}$ for $Sm_xCa_yCe_{1-x-y}O_{2-\delta}$

$CeO_{2-\delta}$		$Sm_xCe_{1-x}O_{2-\delta}$			$Sm_xCa_yCe_{1-x-y}O_{2-\delta}$			
δ	E_{Vo}	x	δ	$E_{Vo\text{-}Sm}$	x	y	δ	$E_{Vo\text{-}CaSm}$
0.0312	2.57	0.0312	0.0312	1.91	0.0312	0.0312	0.0312	–1.56
			0.0625	5.21			0.0625	–1.04
0.0625	2.56	0.0625	0.0625	0.11	0.0625	0.0625	0.0625	–4.18
			0.125	1.84			0.125	–1.53
0.125	2.81	0.125	0.125	1.19	0.125	0.125	0.125	–4.64
			0.250	1.88			0.250	0.01
0.250	3.66	0.250	0.250	1.82	0.250	0.250	0.250	–0.54
			0.50	5.56			0.50	3.08

Oxygen vacancy formation energies of E_{Vo} for $CeO_{2-\delta}$ systems, E_{Vo-Sm} for $Sm_xCe_{1-x}O_{2-\delta}$ systems and $E_{Vo-CaSm}$ for $Sm_xCa_yCe_{1-x-y}O_{2-\delta}$ systems are listed in Table 1. E_{Vo} monotonously increases with increasing δ, see Table 1 and Fig. 3. For $Sm_xCe_{1-x}O_{2-\delta}$ and $Sm_xCa_yCe_{1-x-y}O_{2-\delta}$ systems, we can find that E_{Vo-Sm} with a certain x and $E_{Vo-CaSm}$ with certain x and y are large as δ is large, and both with a certain δ are small as x or x and y are large, see Table 1 and Fig. 3. It need point out that the introduction of Ca and Sm makes the oxygen vacancy spontaneously form, similar to Fergus's study on the Sm-doped CeO_2 systems[49].

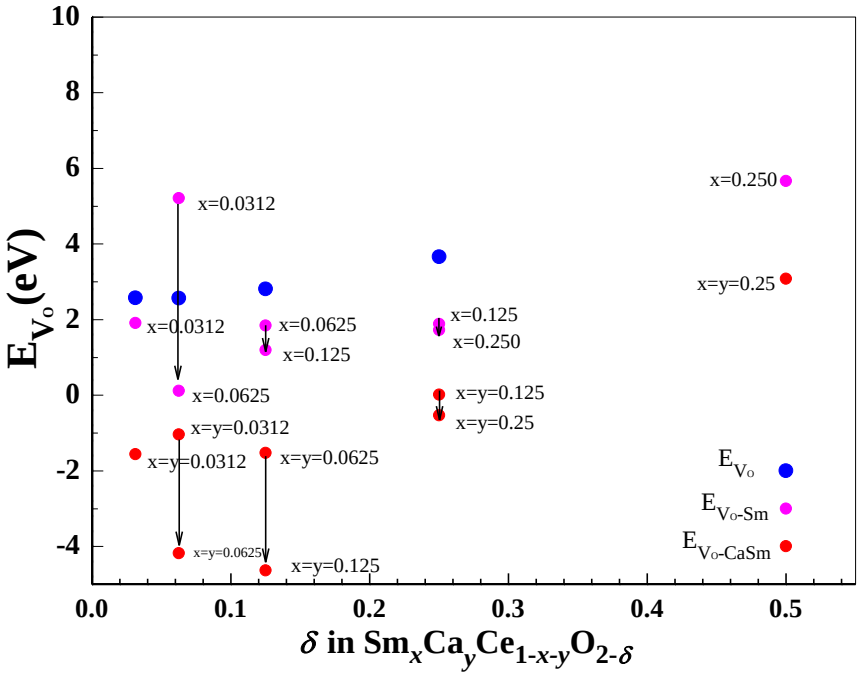

Fig. 3. Variation of E_{Vo}, E_{Vo-Sm}, and $E_{Vo-CaSm}$ as δ of corresponding $CeO_{2-\delta}$, $Sm_xCe_{1-x}O_{2-\delta}$ and $Sm_xCa_yCe_{1-x-y}O_{2-\delta}$ systems

3. 3 Electronic structures

When oxygen vacancies in CeO_2 are formed, the Ce4*f* state is split into two states: an empty $Ce4f_{empty}$ state and an occupied defect $Ce^{3+}4f_{full}$ state at the range of O2*p* and $Ce4f_{empty}$, consistent with our previous[25] and the other work[32], see Fig. 4. Total electronic densities of states (DOS), partial electronic densities of states (PDOS) and localization electronic densities of states (LDOS) from the defect state of Ce^{3+} for various $Sm_xCa_yCe_{1-x-y}O_{2-\delta}$ systems with different x, y and δ are calculated, as shown in Figs. 4 and 5.

3. 3. 1 Excess electron distribution

From the PDOS of Ce4*f* state for $CeO_{1.9688}$, $CeO_{1.9375}$, $CeO_{1.875}$ and $CeO_{1.75}$ systems in Fig. 4a, we can see that a new peak appears at the range of –1.2～0 eV for $CeO_{1.9688}$, $CeO_{1.9375}$, $CeO_{1.875}$ systems and –0.80～0.60 eV for the $CeO_{1.75}$ system, respectively, which are fully occupied by Ce^{3+} electrons. Compared to the

PDOS of Ce4*f* state for the $CeO_{1.75}$ system, the Fermi level of the other systems approximately shift up by 0.50 eV, due to the decrease of oxygen vacancy concentration. Excess electrons arise from the oxygen vacancy and are localized on the *f*-level traps of its neighbor Ce, which can be visually recognized from the corresponding LDOS of the defect Ce^{3+} state in Fig. 4b-e. These are consistent with theoretical studies for $CeO_{1.9843}$, $CeO_{1.9687}$, $CeO_{1.9375}$ and $CeO_{1.875}$[43] and CeO_2(111), (110) and (100) surfaces[50].

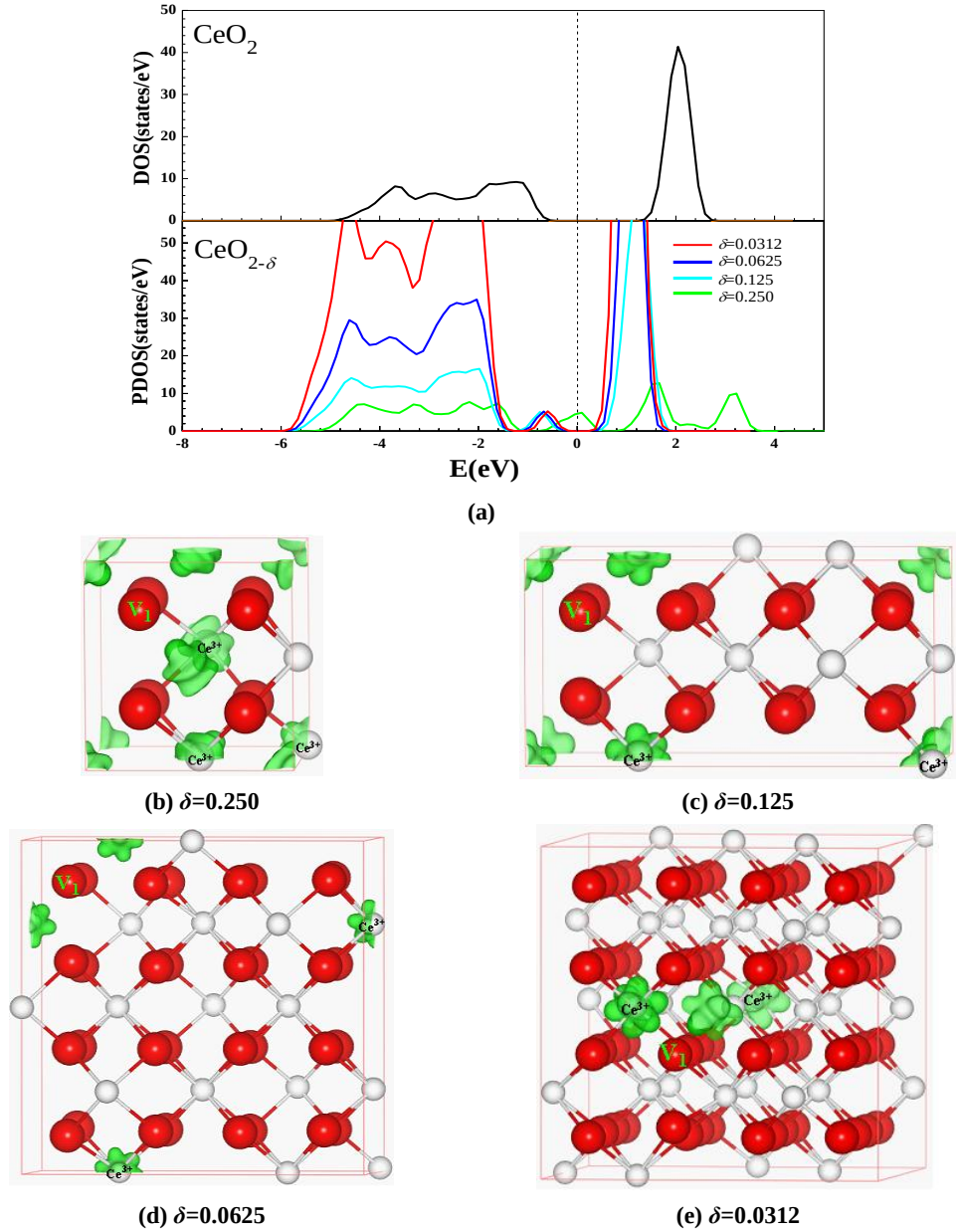

Fig. 4. DOS of the CeO_2 systems and PDOS of Ce4*f* state for $CeO_{1.9688}$, $CeO_{1.9375}$, $CeO_{1.875}$ and $CeO_{1.75}$ systems (a) and the corresponding LDOS (b)-(e) of the defect peaks. The isosurface is shown in green and is set to 0.05 e/Å. Here, one primitive cell of various $CeO_{2-\delta}$ systems with a 2 × 2 × 2 supercell is shown

From the PDOS of Ce4*f* state for $Sm_xCe_{1-x}O_{2-\delta}$ ($0.0312 \leqslant x \leqslant 0.25$, $0.0312 \leqslant \delta \leqslant 0.5$) systems, see Fig. 5a,

similar to $CeO_{2-\delta}$ systems mentioned above, a new peak appears in the range of O2p～Ce4f_{empty}. From the corresponding LDOS of the defect Ce^{3+} state, see Fig. 5c-j, we can see that excess electrons arise from oxygen vacancies and are localized on f-level traps of their neighbor Ce, like the case of $CeO_{2-\delta}$ systems[5, 26, 30, 32]. For the $Sm_{0.0312}Ce_{0.9688}O_{1.9375}$ system, see Fig. 5j, there are two oxygen vacancies in the 2×2×2 supercell, so they should induce four charge-compensation cations. However, the calculated result finds that there are three, maybe due to the existence of V_1-Sm^{3+}-V_2 structure with a face diagonal position relationship in lower reduced atmosphere and then doped Sm^{3+} can restrain the reduction of Ce^{4+}.

In order to better restrain excess electrons, $Sm_xCa_yCe_{1-x-y}O_{2-\delta}$ ($0.0312 \leqslant x \leqslant 0.25$, $0.0312 \leqslant y \leqslant 0.25$, $0.0312 \leqslant \delta \leqslant 0.5$) systems with various x, y and δ are explored. From the DOS of Fig. 5b of $Sm_xCa_yCe_{1-x-y}O_{2-\delta}$ systems, we can see that, except for the $Sm_{0.0625}Ca_{0.0625}Ce_{0.875}O_{1.875}$ system, $Sm_xCa_yCe_{1-x-y}O_{2-\delta}$ systems have no Ce^{3+}. In other words, in order to avoid the existence of Ce^{3+}, x and y must be respectively larger than 0.0625 as δ = 0.125 or δ must be smaller than 0.125 as x = y = 0.0625. For a series of $Sm_xCa_yCe_{1-x-y}O_{2-\delta}$ systems, from their corresponding LDOS of the defect Ce^{3+} state in Fig. 5c-k, we can see that excess electrons arise from oxygen vacancies and are localized on f-level traps of their neighbor Ce, like the case of $CeO_{2-\delta}$[5, 26, 30, 32].

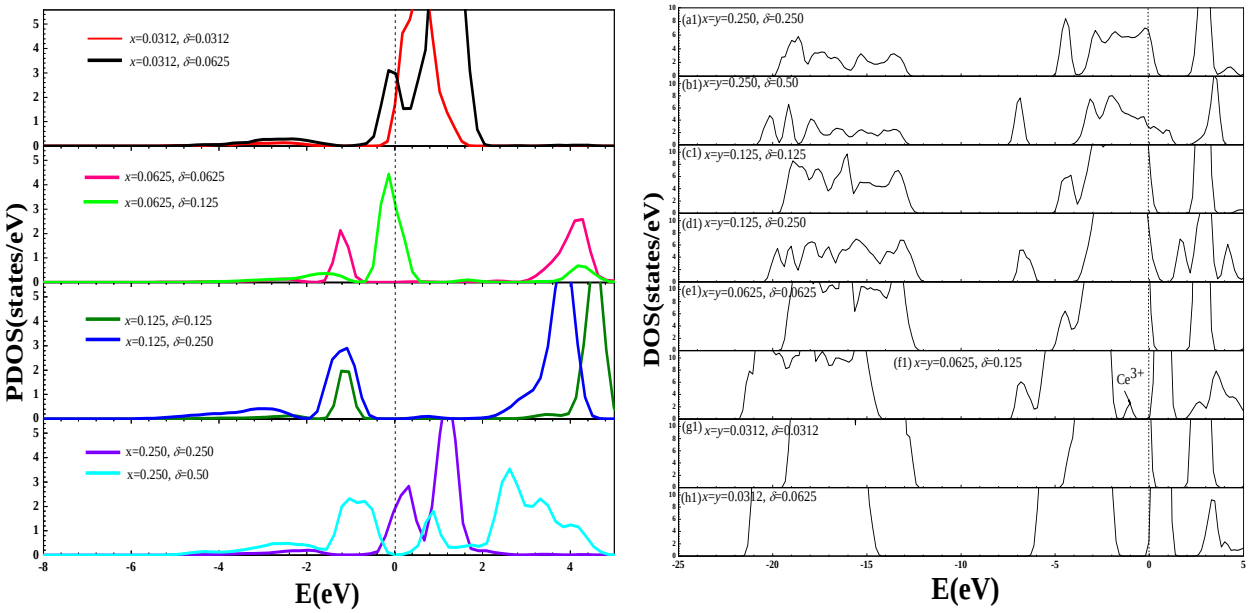

(a) **(b)**

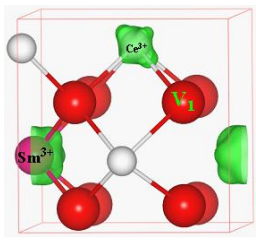

(c) x = 0.250, δ = 0.250

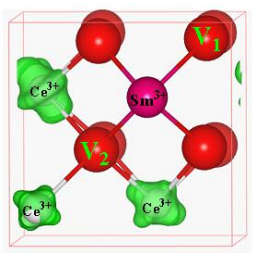

(d) x = 0.250, δ = 0.50

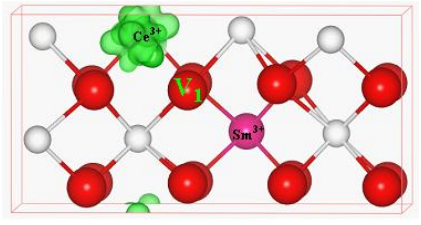

(e) x = 0.125, δ = 0.125

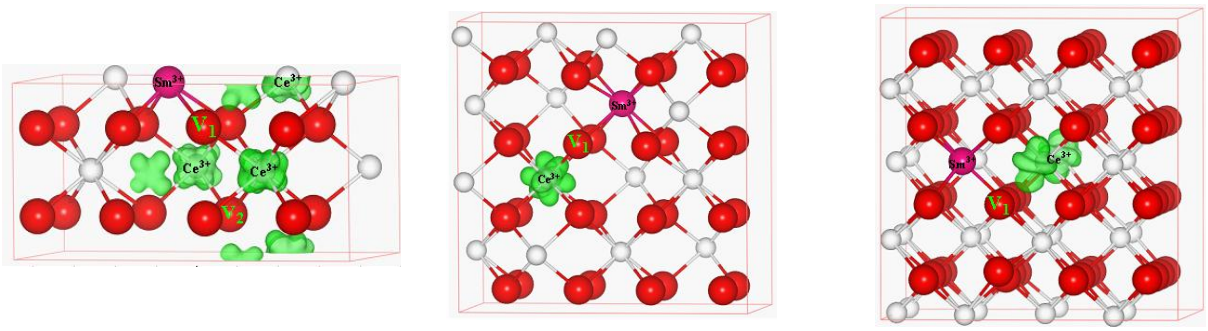

(f) x **= 0.125,** δ **= 0.250** **(g)** x **= 0.0625,** δ **= 0.0625** **(h)** x **= 0.0312,** δ **= 0.0312**

(i) x **= 0.0625,** δ **= 0.125** **(j)** x **= 0.0312,** δ **= 0.0625** **(k)** $x = y$ **= 0.0625,** δ **= 0.125**

Fig. 5. PDOS of Ce4*f* states for the $Sm_xCe_{1-x}O_{2-\delta}$ ($0.0312 \leqslant x \leqslant 0.25$, $0.0312 \leqslant \delta \leqslant 0.5$) systems (a) and DOS of $Sm_xCa_yCe_{1-x-y}O_{2-\delta}$ ($0.0312 \leqslant x \leqslant 0.25$, $0.0312 \leqslant y \leqslant 0.25$, $0.0312 \leqslant \delta \leqslant 0.5$) systems (b) and the corresponding LDOS (c)～(k) of the defect peaks. Oxygen vacancies are represented by V_1 and V_2. The isosurface is shown in green and set to 0.05 e/Å

3. 3. 2 Transitional area of Ce^{4+} to Ce^{3+} and Ce^{3+}/Ce^{4+} change ratio k for $Sm_xCa_yCe_{1-x-y}O_{2-\delta}$ systems with different oxygen vacancy and doping concentrations

In order to visually understand transitional area of Ce^{4+} to Ce^{3+} for the $Sm_xCa_yCe_{1-x-y}O_{2-\delta}$ systems with various oxygen vacancy and doping concentrations, their transitional areas of Ce^{4+} to Ce^{3+} for the $Sm_xCe_{1-x}O_{2-\delta}$ (Fig. 6a) and the $Sm_xCa_yCe_{1-x-y}O_{2-\delta}$ systems (Fig. 6b) are plotted.

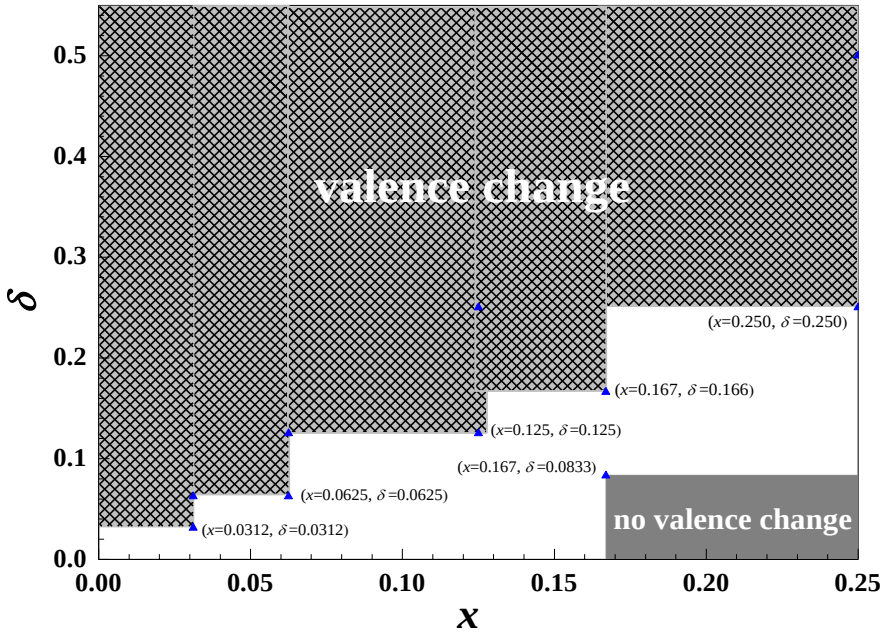

(a)

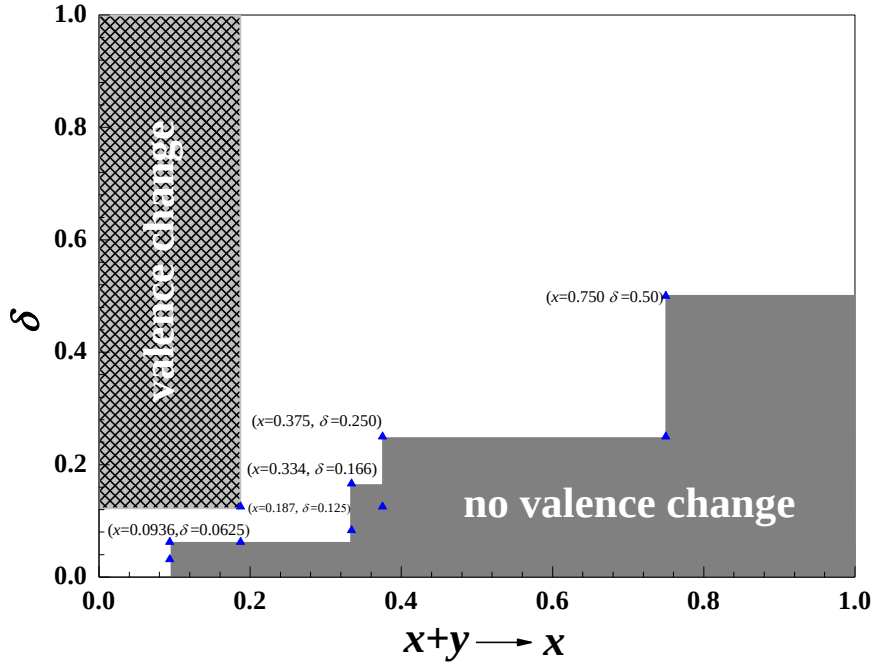

(b)

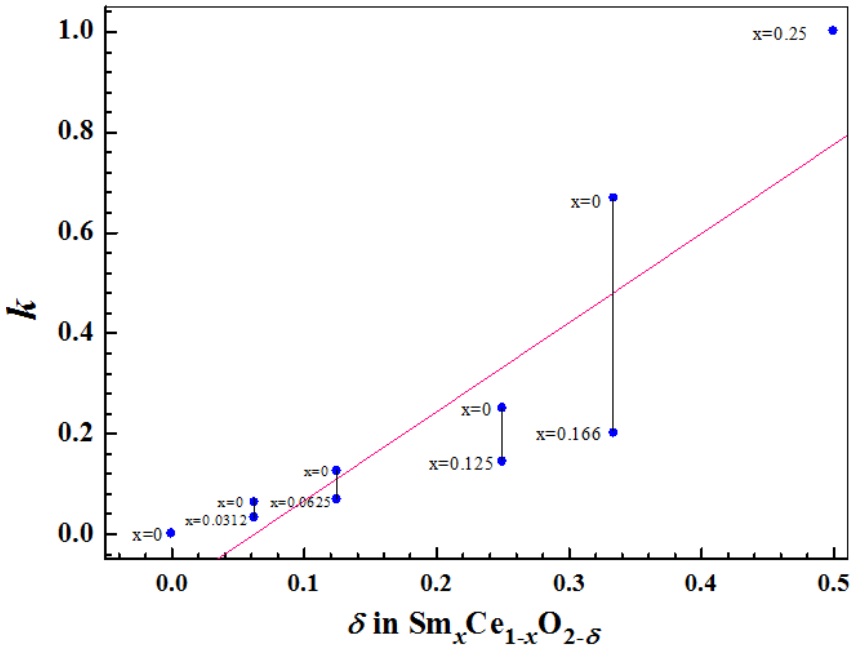

(c)

Fig. 6. Transitional area of Ce^{4+} to Ce^{3+} and Ce^{3+}/Ce^{4+} change ratio *k* for $Sm_xCe_{1-x}O_{2-\delta}$ and $Sm_xCa_yCe_{1-x-y}O_{2-\delta}$ systems with different oxygen vacancy and doping concentrations

From Fig. 6a, we can see that no Ce^{3+} exists for the $Sm_xCe_{1-x}O_{2-\delta}$ systems with $x \geqslant 0.167$ and $\delta \leqslant 0.0833$ and Ce^{3+} exists for the $Sm_xCe_{1-x}O_{2-\delta}$ systems with $x \leqslant 0.0312$ and $\delta \geqslant 0.0312$, $x \leqslant 0.0625$ and $\delta \geqslant 0.0625$, $x \leqslant 0.125$ and $\delta \geqslant 0.125$, $x \leqslant 0.167$ and $\delta \geqslant 0.166$, and $x \leqslant 0.250$ and $\delta \geqslant 0.250$. For the $Sm_xCa_yCe_{1-x-y}O_{2-\delta}$ system as $y \neq 0$, the substitution of Ce^{4+} by Ca^{2+} makes two excess electrons and the substitution of Ce^{4+} by Sm^{3+} makes one excess electron. Based on the case, for convenience of totally reflecting the effect of the doping concentration on the transition ratio of Ce^{4+} to Ce^{3+}, the doping effect of one Ca^{2+} is transformed to that of two Sm^{3+}, in which the ionic radius of doping Ca^{2+} and Sm^{3+} is omitted, and its corresponding transitional area of Ce^{4+} to Ce^{3+} is plotted in Fig. 6b. From Fig. 6b, we can see that no Ce^{3+} exists for the $Sm_xCa_yCe_{1-x-y}O_{2-\delta}$ systems with $x \geqslant 0.0936$ and $\delta \leqslant 0.0625$, $x \geqslant 0.334$ and $\delta \leqslant 0.166$, $x \geqslant 0.375$ and $\delta \leqslant 0.250$, and $x \geqslant 0.750$ and $\delta \leqslant 0.50$ and Ce^{3+} exists for the $Sm_xCa_yCe_{1-x-y}O_{2-\delta}$ systems with $x \leqslant 0.187$ and $\delta \geqslant 0.125$.

The Ce^{3+}/Ce^{4+} change ratio *k* in $Sm_xCe_{1-x}O_{2-\delta}$ systems with various oxygen vacancy and doping concentrations are studied, as shown in Fig. 6c. From Fig. 6c, we can see that *k* has obvious monotonous increase with increasing the vacancy concentration, and the introduction of Sm^{3+} reduces *k*, such as $Sm_{0.0312}Ce_{0.9688}O_{1.9375}$, $Sm_{0.0625}Ce_{0.9375}O_{1.875}$, $Sm_{0.125}Ce_{0.875}O_{1.75}$, $Sm_{0.166}Ce_{0.834}O_{1.668}$ and $Sm_{0.25}Ce_{0.75}O_{1.5}$ systems, namely, the introduction of Sm^{3+} restrains the reduction of Ce^{4+} to Ce^{3+}. It need be pointed out that

$Sm_{0.25}Ce_{0.75}O_{1.5}$ system can be thought of as Sm-doped Ce_2O_3, because of no unoccupied defect states between the occupied Ce^{3+} states and the unoccupied Ce4f_{empty}, see Fig. 5a, in accordance with other theoretical work[51-53].

4 CONCLUSION

In this work, the influence of Sm^{3+} single-doping or Ca^{2+} and Sm^{3+} co-doping, oxygen vacancies and their concentrations on the geometric and electronic structures of $Sm_xCa_yCe_{1-x-y}O_{2-\delta}$ systems are studied. Results for the geometric structures show that the V_1-Sm^{3+}-V_2 structures where there is a position relationship of diagonal of the face between V_1 and V_2 both nearest to Sm^{3+} are easily obtained, in agreement with the case of pure CeO_2 systems. Study for electronic structures finds that the oxygen vacancies are contributed to excess electrons and these electrons are localized on *f*-level traps of its neighbor Ce for the $Sm_xCa_yCe_{1-x-y}O_{2-\delta}$ systems. The Ce^{3+}/Ce^{4+} change ratio *k* is related with the dopant and oxygen vacancy concentrations. In addition, the existence of V_1-Sm^{3+}-V_2 structure with face diagonal position relationship in lower reduced atmosphere maybe makes the doped Sm^{3+} restrain the reduction of Ce^{4+}. It need be pointed out that $Sm_{0.25}Ce_{0.75}O_{1.5}$ system can be thought of as Sm-doped Ce_2O_3.

REFERENCES

(1) Brett, D. J. L.; Atkinson, A.; Brandon, N. P.; Skinner, S. J. Intermediate temperature solid oxide fuel cells. *Chem. Soc. Rev.* **2008**, 37, 1568–1578.

(2) Ruiz, T. E.; Sirman, J. D.; Baikov, Y. M.; Kilner, J. A. Oxygen ion diffusivity, surface exchange and ionic conductivity in single crystal Gadolinia doped Ceria. *Solid State Ionics* **1998**, 113, 565–569.

(3) Park, S.; Vohs, J. M.; Gorte, R. J. Direct oxidation of hydrocarbons in a solid-oxide fuel cell. *Nature* (*London*) **2000**, 404, 265–267.

(4) Molinari, M.; Parker, S. C.; Sayle, D. C.; Islam, M. S. Water adsorption and its effect on the stability of low index stoichiometric and reduced surfaces of ceria. *J. Phys. Chem. C* **2012**, 116, 7073–7082.

(5) Kullgren, J.; Hermansson, K.; Castleton, C. Many competing ceria(110) oxygen vacancy structures: from small to large supercells. *J. Chem. Phys.* **2012**, 137, 044705.

(6) Allen, J. P.; Watson, G. W. Occupation matrix control of *d*- and *f*-electron localisations using DFT + *U*. *Phys. Chem. Chem. Phys.* **2014**, 16, 21016–21031.

(7) Steele, B. C. H. Appraisal of $Ce_{1-y}Gd_yO_{2-y/2}$ electrolytes for IT-SOFC operation at 500 ℃. *Solid State Ionics* **2000**, 129, 95–110.

(8) Ismail, A.; Hooper, J.; Giorgi, J. B. A DFT + U study of defect association and oxygen migration in samarium-doped ceria. *Phys. Chem. Chem. Phys.* **2011**, 13, 6116–6120.

(9) Suparna, B.; Parukuttyamma, S. D.; Dinesh, T. S. M.; Krishnakumar, M. Enhanced ionic conductivity in $Ce_{0.8}Sm_{0.2}O_{1.9}$: unique effect of calcium Co-doping. *Adv. Funct. Mater.* **2007**, 17, 2847–2854.

(10) Wang, F. Y.; Cheng, S. Gd^{3+} and Sm^{3+} co-doped ceria based electrolytes for intermediate temperature solid oxide fuel cells. *Electrochem. Commun.* **2004**, 6, 743–746.

(11) Kim, N.; Kim, B. H.; Lee, D. Effect of co-dopant addition on properties of gadolinia-doped ceria electrolyte. *J. Power Sources* **2000**, 90, 139–143.

(12) Mori, T.; Yamamura, H. Preparation of an alkali-element or alkali-earth-element-doped CeO_2-Sm_2O_3 system and its operation properties as the electrolyte in planar solid oxide fuel cells. *J. Mater. Synth. Process.* **1998**, 6, 175–179.

(13) Van, H. J.; Horita, T.; Kawada, T.; Sakai, N.; Yokokawa, H. Low temperature fabrication of (Y, Gd, Sm)-doped ceria electrolyte. *Solid State Ionics* **1996**, 86, 1255–1258.

(14) Yang, N.; Belianinov, A.; Strelcov, E. Effect of doping on surface reactivity and conduction mechanism in samarium-doped ceria thin films. *ACS nano* **2014**, 8, 12494–12501.

(15) Ruiz-Trejo, E.; Sirman, J. D.; Baikov, Y. M.; Kilner, J. A. Nanoparticles and nanoceramics of Y-doped CeO_2. *Solid State Ionics* **1998**, 113, 565–571.

(16) Yoshida, H.; Deguchi, H.; Miura, K. Investigation of the relationship between the ionic conductivity and the local structures of singly and doubly doped ceria compounds using EXAFS measurement. *Solid State Ionics* **2001**,140, 191–199.

(17) Andersson, D. A.; Simak, S. I.; Skorodumova, N. V. Optimization of ionic conductivity in doped ceria. *Proc. Natl. Acad. Sci. USA* **2006**, 103, 3518–3521.

(18) Yin, Y. H.; Li, S. Y.; Zhu, W.; Xia, C. R. Research on calcium-doped ceria used in intermediate-temperature SOFCs anodes. *J. Chin. Rare Earth Soc.* **2005**, 03, 317–322.

(19) Mogensen, M.; Lindegaard, T.; Hansen, U. R. Physical properties of mixed conductor solid oxide fuel cell anodes of doped CeO_2. *J. Electrochem. Soc.* **1994**, 141, 2122–2126.

(20) Wei, X.; Pan, W.; Cheng, L. Atomistic calculation of association energy in doped ceria. *Solid State Ionics* **2009**, 180, 13–17.

(21) Frayret, C.; Villesuzanne, A.; Pouchard, M.; Matar, S. Density functional theory calculations on microscopic aspects of oxygen diffusion in ceria-based materials. *Int. J. Quantum Chem.* **2005**, 101, 826–839.

(22) Nakayama, M.; Martin, M. First-principles study on defect chemistry and migration of oxide ions in ceria doped with rare-earth cations. *Phys. Chem. Chem. Phys.* **2009**, 11, 3241–3249.

(23) Grinter, D. C.; Ithnin, R.; Pang, C. L.; Thorton, G. Defect structure of ultrathin ceria films on Pt(111): atomic views from scanning tunneling microscopy. *J. Phys. Chem. C* **2010**, 114, 17036–17041.

(24) Nolan, M.; Fearon, J. E.; Watson, G. W. Oxygen vacancy formation and migration in ceria. *Solid State Ionics* **2006**, 177, 3069–3074.

(25) Jia, G. X.; Hao, W. X.; Pan, F.; Yang, J. C.; Zhang, Y. F. Electronic structures and oxygen ion migration energies of metal doped CeO_2 systems: a DFT ＋*U* study. *Acta Chim. Sinica* **2013**, 71, 1668–1675.

(26) Wu, T. W.; Jia, G. X.; Bao, J. X.; Liu, Y. Y.; An, S. L. Electronic structures and oxygen ion migrations of the CaO or BaO and Sm_2O_3 co-doped CeO_2 System: A DFT + U Study. *Chin. J. Inorg. Chem.* **2016**, 32, 1363–1369.

(27) Yahiro, H.; Eguchi, K.; Arai, H. Electrical properties and reducibilities of ceria-rare earth oxide systems and their application to solid oxide fuel cell. *Solid Stale Ionics* **1989**, 36, 71–75.

(28) Kumar, A.; Devi, P. S.; Maiti, H. S. A novel approach to develop dense lanthanum calcium chromite sintered ceramics with very high conductivity. *Chem. Mater.* **2004**, 16, 5562–5563.

(29) Banerjee, S. P.; Devi, S. Sinter-active nanocrystalline CeO_2 powder prepared by a mixed fuel process: effect of fuel on particle agglomeration. *J. Nanoparticle Res.* **2007**, 9, 1097–1107.

(30) Murgida, G. E.; Ferrari, V.; Ganduglia, P. M. V. Ordering of oxygen vacancies and excess charge localization in bulk ceria: a DFT + U study. *Phys. Rev. B* **2014**, 90, 115120/1–10.

(31) Zhang, C.; Michaelides, A.; King, D. A.; Jenkins, S. J. Oxygen vacancy clusters on ceria: decisive role of cerium *f* electrons. *Phys. Rev. B* **2009**, 79, 075433/1–11.

(32) Graciani, J.; Antonio, M.; Márquez, J. J.; Plata, Y. O.; Norge, C.; Meyer, H. A.; Claudio, M.; Zicovich, W.; Javier, F. S. Comparative study on the performance of hybrid DFT functionals in highly correlated oxides: the case of CeO_2 and Ce_2O_3. *J. Chem. Theory Comput.* **2011**, 7, 56–65.

(33) Hooper, J.; Ismail, A.; Giorgi, J. B. Computational insights into the nature of increased ionic conductivity in concentrated samarium-doped ceria: a genetic algorithm study. *Phys. Chem. Chem. Phys.* **2010**, 12, 12969–12972.

(34) Kresse, G.; Furthmüller, J. Efficiency of *ab-initio* total energy calculations for metals and semiconductors using a plane-wave basis set. *Comput. Mater. Sci*. **1996**, 6, 15–50.

(35) Delfina, G. P.; Alfredo, J.; Beatriz, I. Mn-doped CeO_2: DFT + U study of a catalyst for oxidation reactions. *J. Phys. Chem. C* **2013**, 117, 18063–18073.

(36) Perdew, J. P.; Burke, K.; Ernzerhof, M. Generalized gradient approximation made simple. *Phys. Rev. Lett.* **1996**, 77, 3865–3867.

(37) Castleton, C. W.; Kullgren, J.; Hermansson, K. Tuning LDA+U for electron localization and structure at oxygen vacancies in ceria. *J. Chem. Phys.* 2007, 127, 244704/1–11.

(38) Loschen, C.; Carrasco, J.; Neyman, K. M. Illas, F. First-principles LDA+U and GGA+U study of cerium oxides: Dependence on the effective U parameter. *Phys. Rev. B* 2007, 75, 035115/1–8.

(39) Nolan, M.; Parker, S. C.; Watson, G. W. Reduction of NO2 on ceria surfaces. *J. Phys. Chem. B* 2006, 110, 2256–2262.

(40) Nolan, M.; Watson, G. W. The surface dependence of CO adsorption on ceria. *J. Phys. Chem. B* **2006**, 110, 16600–16606.

(41) Nolan, M.; Parker, S. C.; Watson, G. W. CeO_2 catalysed conversion of CO, NO_2 and NO from first principles energetics. *Phys. Chem. Chem. Phys.* **2006**, 8, 216–218.

(42) Scanlon, D. O.; Galea, N. M.; Morgan, B. J.; Watson, G. W. Reactivity on the (110) surface of ceria: a GGA+*U* study of surface reduction and the adsorption of CO and NO_2. *J. Phys. Chem. C* **2009**, 113, 11095–11103.

(43) Keating, P. R. L.; Scanlon, D. O.; Watson, G. W. Intrinsic ferromagnetism in CeO_2: dispelling the myth of vacancy site localization mediated superexchange. *J. Phys. Condens. Mat.* **2009**, 21, 405502/1–6.

(44) Dudarev, S. L.; Botton, G. A.; Savrasov, S. Y.; Humphreys, C. J.; Sutton, A. P. Surface proton hopping and fast-kinetics pathway of water oxidation on Co_3O_4 (001) surface. *Phys. Rev. B* **1998**, 57, 1505–1517.

(45) Larson, P. W.; Lambrecht, R. L.; Chantis, A. N.; Schilfgaarde, V. M. Electronic structure of rare-earth nitrides using the LSDA+*U* approach: importance of allowing 4*f* orbitals to break the cubic crystal symmetry. *Phys. Rev. B* **2007**, 75, 045114/1–14.

(46) Dorado, B.; Jomard, G.; Freyss, M.; Bertolus, M. Stability of oxygen point defects in UO_2 by first-principles DFT + U calculations: occupation matrix control and Jahn-Teller distortion. *Phys. Rev. B* **2010**, 82, 035114/1–11.

(47) Feng, J.; Xiao, B.; Wan, C. L. Electronic structure, mechanical properties and thermal conductivity of $Ln_2Zr_2O_7$ (Ln = La, Pr, Nd, Sm, Eu and Gd) pyrochlore. *Acta Mater.* **2011**, 59, 1742–1760.

(48) Monkhorst, H. J.; Pack, J. D. Special points for Brillouin-zone integrations. *Phys. Rev. B* **1976**, 13, 5188–5192.

(49) Fergus, J. W. Recent developments in cathode materials for lithium ion batteries. *J. Power Sources* **2006**, 189, 30–36.

(50) Nolan, M.; Parker, S. C.; Watson, G. W. The electronic structure of oxygen vacancy defects at the low index surfaces of ceria. *Surf. Sci.* **2005**, 595, 223–232.

(51) Silva, D. G. L. F.; Ganduglia, P. M. V.; Sauer, J.; Bayer, V.; Kresse, G. Hybrid functionals applied to rare-earth oxides: the example of ceria. *Phys. Rev. B* **2007**, 75, 045121/1–10.

(52) Skorodumova, N. V.; Ahuja, R.; Simak, S. I.; Abrikosov, A.; Johansson, B.; Lundqvist, B. I. Electronic, bonding, and optical properties of CeO_2 and Ce_2 O_3 from first principles. *Phys. Rev. B* **2001**, 64, 115108/1–9.

(53) Andersson, D. A.; Simak, S. I.; Johansson, B.; Abrikosov, I. A.; Skorodumova, N. V. Modeling of CeO_2, Ce_2O_3, and CeO_{2-x} in the LDA+*U* formalism. *Phys. Rev. B* **2007**, 75, 035109/1–6.

Transitional Area of Ce^{4+} to Ce^{3+} in $Sm_xCa_yCe_{1-x-y}O_{2-\delta}$ with Various Doping and Oxygen Vacancy Concentrations: A GGA + *U* Study

WU Tong-Wei(吴铜伟)　JIA Gui-Xiao(贾桂霄)

WANG Xiao-Xia(王晓霞)　LI Lei(李磊)　AN Sheng-Li(安胜利)

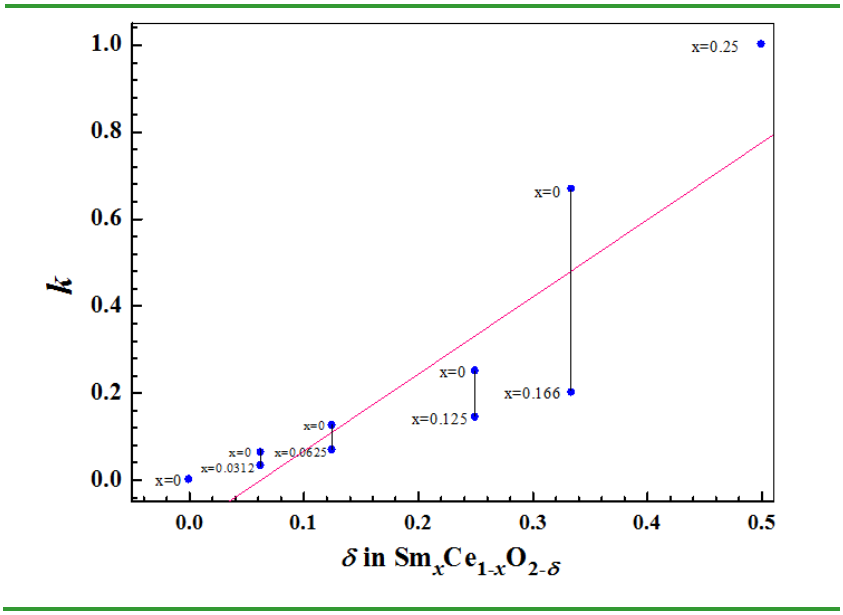

The Ce^{3+}/Ce^{4+} change ratio *k* has obvious monotonous increase with increasing the vacancy concentration. The introduction of Sm^{3+} reduces *k*. It need be pointed out that the $Sm_{0.25}Ce_{0.75}O_{1.5}$ system can be thought of as Sm-doped Ce_2O_3.